Proceeding of International Joint Conference on UNESA
Homepage : https://proceeding.unesa.ac.id/index.php/pijcu
ISSN : 3032 - 3762

PIJCU, Vol. 3, No. 1, Desember 2025
Page 872 - 880

Analysis of Material and Wavelength Effects on Optical Propagation Performance in Dual Parallel Symmetric Mach-Zehnder Interferometer (DPS-MZI) Structures Using OptiBPM

Nisa'ul Fadhilah[1], Riski Ramadani[1], Afiyah Nikmah[1], Muhammad Bagoes Anargiansyah[1], Muhimmatul Khoiro[1*]
[1*] Physics Department, Universitas Negeri Surabaya, Surabaya, Indonesia

Keywords:
Mach-Zehnder Interferometer
Beam Propagation Methods
Optical Waveguide
Propagation Loss
Materials

ABSTRACT

Innovations in integrated photonic technology have increased the demand for compact and high-performance optical devices. The MZI (Mach Zender Inferferometer) is a key component, particularly the DPS-MZI structure, which offers flexibility in optical signal processing, spectral filtering, and high-precision sensing applications. This study analyses the optical characteristics and performance of DPS-MZI structures based on four waveguide core materials of Si, InGaAsP, $LiNbO_3$, and PMMA, at wavelengths of 532 nm, 633 nm, 850 nm, and 1550 nm. Simulations were conducted using the OptiBPM software, which employs the BPM, to evaluate optical field intensity distribution, interference patterns, and propagation losses. The results indicate that Si and InGaAsP exhibit the best propagation performance, with low power loss and sharp interference patterns, while $LiNbO_3$ experiences higher propagation losses despite its high electro-optic coefficient. PMMA demonstrates the lowest performance due to its low refractive index contrast, leading to significant light spreading into the cladding and high propagation losses. An increase in wavelength tends to broaden the optical mode, particularly in materials with low refractive index contrast. This study underscores the importance of selecting appropriate waveguide core materials and operating wavelengths when designing DPS-MZI-based photonic devices to ensure stable and efficient light propagation.

INTRODUCTION

The advancement of integrated photonic technology continues to drive the demand for high-performance optical devices with increasingly compact dimensions. One of the fundamental components widely utilized is the Mach-Zehnder Interferometer (MZI), due to its ability to manipulate the phase and intensity of light through optical interference phenomena (Chen et al., 2022; Zhu et al., 2025). The Dual Parallel Symmetric MZI (DPS-MZI) structure has emerged as an innovative solution, offering flexibility in optical signal processing, spectral filtering, and high-precision sensing applications (Dong et al., 2020; Yang et al., 2024). In the DPS-MZI configuration, two identical MZIs are arranged in a parallel and symmetric layout, enabling more complex interference responses, sidelobe suppression, and a higher extinction ratio compared to a single MZI (Amin et al., 2020).
Material selection is a crucial factor in the design of DPS-MZI, as optical characteristics such as refractive index, electro-optic coefficient, and spectral transparency significantly influence device performance. Silicon (Si) remains the primary material in integrated photonic technology due to its compatibility with CMOS (Complementary Metal-Oxide-Semiconductor) processes and its excellent light-confining ability, with a refractive index of approximately 3.47 at a wavelength of 1550 nm, making it well-suited for operation in the telecommunications spectrum (Siew et al., 2021; Kim et al., 2020; Dong et al., 2024;

Tsuda et al., 2020). Nevertheless, silicon has inherent limitations in its electro-optic response, making it less ideal for applications requiring high-speed direct modulation. On the other hand, Indium Gallium Arsenide Phosphide (InGaAsP) is widely used in optical communication windows of 1.3-1.55 μm due to its advantages in active applications such as optical modulation and amplification, and its ability to integrate with III–V photonic platforms suitable for optoelectronic systems (Moatlhodi, 2022; Hiraki et al., 2020; Vyas et al., 2022). Lithium Niobate ($LiNbO_3$) is well-known for its high electro-optic coefficient, enabling efficient conversion of electrical signals into optical signals, making it highly suitable for high-speed modulators. However, the integration of $LiNbO_3$ into compact silicon-based technologies still faces significant technical challenges (Di Francescantonio et al., 2025; Huang et al., 2025; Tu et al., 2025). Meanwhile, Polymethyl methacrylate (PMMA), as a polymeric material with a relatively low refractive index (~1.48), has attracted attention due to its ease of fabrication, low cost, geometric flexibility, and broad spectral transparency including the visible region (532 nm, 633 nm) to the near-infrared. However, PMMA has limitations in thermal stability and optical performance when compared to inorganic materials (Alsaad et al., 2021; Nagar et al., 2024; Zhan et al., 2021; Saxena & Shukla, 2022).

In addition to material selection, the operating wavelength is also a critical aspect in DPS-MZI design. At wavelengths of 532 nm and 633 nm, applications are mainly directed toward biosensing, imaging, and visible light communication systems (Li et al., 2025; Butt, 2024). The 850 nm wavelength is widely used in short-range communication systems and medical optical applications (Prabu et al., 2025; Lorenz & Bock, 2022). Meanwhile, the 1550 nm wavelength has become the standard in optical communication due to its low attenuation in silica optical fibers and its relative eye safety (Sohn et al., 2020; Akbulut et al., 2021). These wavelength variations demand an MZI design capable of maintaining optimal interference performance across a wide spectral range, which heavily depends on the optical properties of the selected materials.

Considering the design complexity, material variation, and wavelength diversity, research on the DPS-MZI structure is highly relevant to addressing current challenges in photonic device development, whether for communication, signal processing, or high-precision optical sensing applications. This study aims to analyze the optical characteristics and performance of the Dual Parallel Symmetric MZI structure using four different materials at various wavelengths, thereby providing insights for designing more efficient and multifunctional photonic devices.

RESEARCH METHOD

This research was conducted using the OptiBPM software, which is based on the Beam Propagation Method (BPM) and is widely used to analyze the behavior of light in planar waveguide structures (Karabchevsky & Choudhary, 2024; Wang et al., 2020). The simulated structure is the DPS-MZI, designed with two identical interferometer arms connected in a parallel and symmetric configuration. The geometry of the DPS-MZI was modeled in such a way as to demonstrate the interference patterns and light intensity distribution generated under various material and wavelength conditions.

This study varies four types of materials as the waveguide core: Silicon (Si) with a refractive index of 3.48, Indium Gallium Arsenide Phosphide (InGaAsP) with a refractive

index of 3.253, Lithium Niobate ($LiNbO_3$) with a refractive index of 2.2592, and Polymethyl methacrylate (PMMA) with a refractive index of 1.49 (Modi et al., 2020; Pan et al., 2021; Yu et al., 2021; Mulkerns et al., 2022). The selection of these materials is based on their distinct optical properties, such as refractive index, dispersion characteristics, and spectral transparency, enabling exploration of how each material affects interference performance within the DPS-MZI. The wavelengths used in the simulations include 532 nm (Green), 633 nm (Red), 850 nm (Near Infrared), and 1550 nm (Infrared), chosen to cover the spectrum from visible to near-infrared light, relevant for various applications in optical communications, optical sensing, and integrated photonic technologies (Poon et al., 2024; Alzamil et al., 2024; Kazanskiy et al., 2022). All simulations were performed with a silica (SiO_2) substrate, which has a refractive index of approximately 1.45 (Modi et al., 2020).

For each variation of material and wavelength, simulations were carried out by defining the geometry of the DPS-MZI, including the waveguide dimensions and the spacing between waveguides in the coupler region, to enable clear analysis of optical interactions between the interferometer paths. Light propagation was simulated along the DPS-MZI structure to observe the optical field intensity distribution, interference patterns, dispersion, transmission loss (insertion loss), as well as bending loss. The simulation results were then analyzed to evaluate the influence of variations in core material refractive index and wavelength on the performance of the DPS-MZI. The outcomes of this research are expected to provide in-depth insights into how material selection and wavelength impact the interference characteristics and overall performance of photonic devices based on the DPS-MZI structure.

RESULTS AND DISCUSSION

Based on simulation results using OptiBPM at a wavelength of 1550 nm, variations in the light intensity distribution patterns were observed within the DPS-MZI structure for each waveguide core material. These differences are caused by the distinct refractive indices and optical properties of each material, which directly influence how light waves propagate within the waveguide. The propagation results can be seen in **Figure 1**.

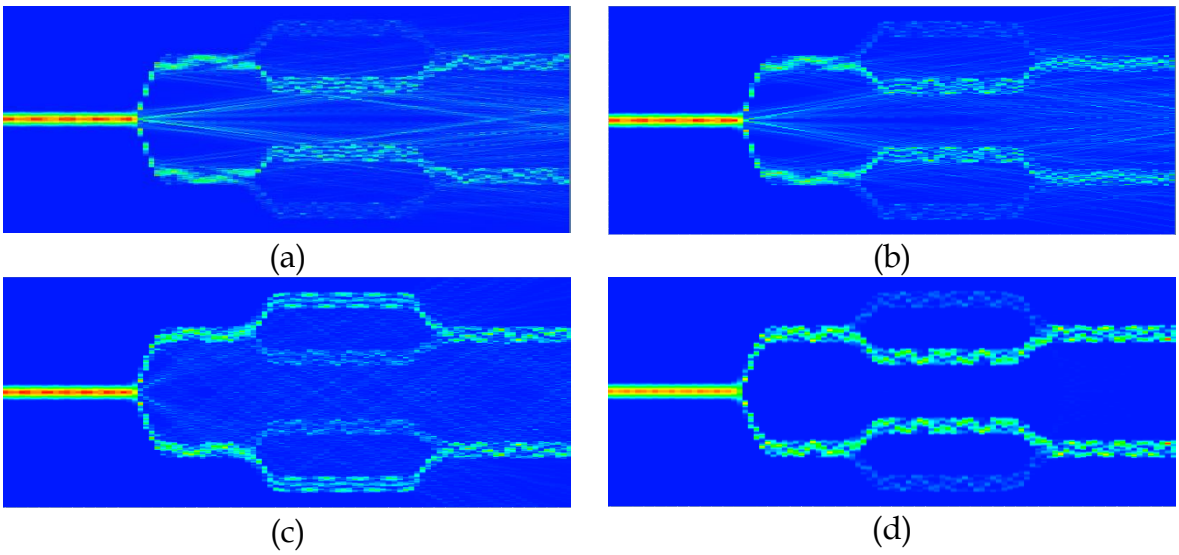

(a) (b) (c) (d)

Figure 1. Optical field propagation in materials (a) Si, (b) InGaAsP, (c) $LiNbO_3$, and (d) PMMA.

Based on **Figure 1**, the optical wave propagation performance is highly influenced by the characteristics of the waveguide materials used. Waveguides made of Si demonstrate excellent optical field confinement due to their high refractive index (~3.47), effectively trapping light within the waveguide core. This results in well-defined interference patterns, high intensity, and low propagation losses, making silicon highly suitable for high-speed optical communication applications (Zhou et al., 2024; Wang et al., 2024). Meanwhile, waveguides made of InGaAsP also exhibit good confinement in the wavelength range of 1.3–1.55 µm, although their output intensity is slightly lower than that of silicon due to their relatively smaller refractive index contrast. Nevertheless, InGaAsP remains advantageous for active applications such as optical modulation and amplification (Horvath et al., 2020). Waveguides composed of $LiNbO_3$ possess the advantage of a high electro-optic coefficient, which is crucial for high-speed modulation applications. However, they show weaker optical field confinement compared to silicon because of their lower refractive index (~2.2), leading to broader interference patterns and reduced intensity (Sun et al., 2022).

In waveguides made of PMMA, it is observed that the light propagation path is clearly visible and follows the geometric shape of the device. However, the clarity of this path does not necessarily indicate good wave propagation performance. This is due to the refractive index of PMMA (~1.48), which is close to that of the cladding or substrate (silica), resulting in a very small refractive index contrast. This condition leads to extremely weak optical field confinement, causing the light to spread more widely into areas surrounding the waveguide core, even though it visually appears to remain within the waveguide path. Consequently, the optical modes become broader and exhibit significant overlap into the cladding, leading to higher propagation losses and reduced interference efficiency, as a portion of the light escapes from the waveguide core (Islam & Ahmed, 2020). Therefore, although the waveguide structure in PMMA is geometrically well-defined, its wave propagation quality and interference patterns exhibit lower performance compared to materials with higher refractive indices.

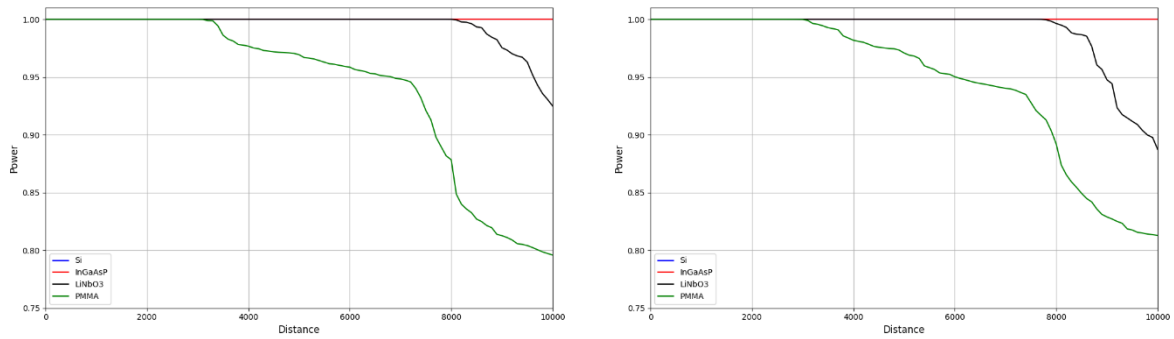

(a) (b)

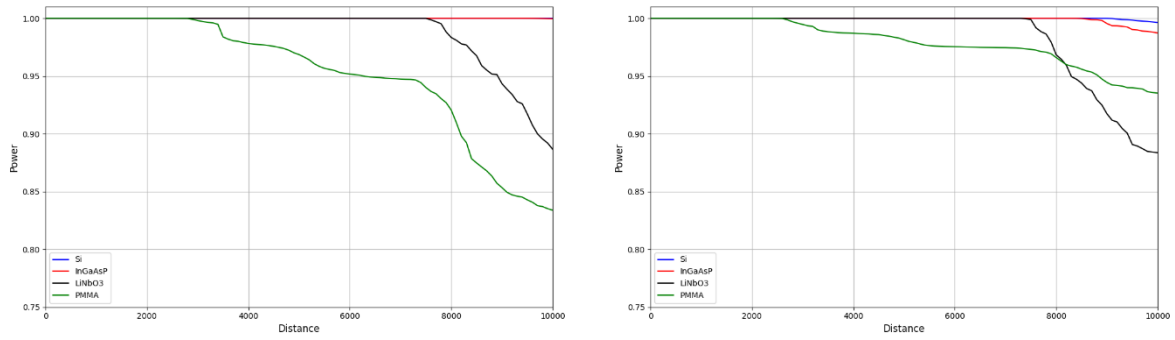

(c) (d)

Figure 2. Relative optical power variation along the propagation path at (a) 532 nm, (b) 633 nm, (c) 850 nm, and (d) 1550 nm.

Furthermore, the results of optical wave propagation simulations are also influenced by the wavelength of light used. Figure 2 presents a comparative graph of optical power versus propagation distance for four wavelengths (532 nm, 633 nm, 850 nm, and 1550 nm). The graph shows a consistent trend in which materials with high refractive indices, such as Silicon (Si) and Indium Gallium Arsenide Phosphide (InGaAsP), exhibit the best propagation performance, while PMMA demonstrates the lowest performance due to high propagation losses.

At a wavelength of 532 nm, Si and InGaAsP are able to maintain optical power close to 100% over a propagation length of 10,000 µm, indicating very low propagation losses and strong optical field confinement. This is attributed to the significant refractive index contrast between the waveguide core and the cladding (silica), which keeps the light effectively confined within the waveguide. Conversely, $LiNbO_3$ begins to show a decrease in power after approximately 8,000 µm, while PMMA experiences significant losses starting from a distance of 4,000 µm, with power dropping to around ~80% at the end of the propagation path. This pattern indicates weak optical confinement in PMMA, causing light to spread into the cladding and resulting in energy loss.

At a wavelength of 633 nm, Si and InGaAsP continue to maintain almost constant optical power. $LiNbO_3$ and PMMA again exhibit a decline, with PMMA suffering sharper losses. Interestingly, at a wavelength of 850 nm, although Si still shows excellent power stability, the curve for InGaAsP begins to show a decrease after 9,000 µm, albeit still within a low tolerance range. Meanwhile, $LiNbO_3$ and PMMA experience greater losses compared to the previous wavelengths. This indicates that increasing the wavelength leads to broader optical mode spreading, especially in materials with low refractive index contrast, such as PMMA and $LiNbO_3$.

At a wavelength of 1550 nm, Si and InGaAsP demonstrate optimal performance with very low losses, maintaining excellent propagation characteristics, strong optical confinement, and nearly stable power levels throughout propagation. In contrast, $LiNbO_3$ and PMMA exhibit significant power reductions. $LiNbO_3$ begins to experience power loss after propagating approximately 7,000 µm. The most drastic power decrease is observed in PMMA from the outset, as its low refractive index leads to light leakage into the cladding.

The consistent power reduction in PMMA across all wavelengths indicates this material's inability to effectively confine light within the waveguide. Therefore, PMMA is less suitable for waveguide applications that require medium to long propagation paths, as light continually loses energy due to leakage into the cladding. Although the interference patterns in PMMA are less well-defined and its intensity is lower compared to silicon-based waveguides, PMMA remains relevant for certain applications, such as evanescent wave-based sensors, owing to its ease of fabrication, low cost, and flexibility in manufacturing waveguide devices with complex geometries. However, PMMA has significant limitations for DPS-MZI applications that require sharp interference and low propagation losses (Kazanskiy et al., 2022; Zhou et al., 2024; Wang et al., 2024).

CONCLUSION

Based OptiBPM simulations indicate that the optical wave propagation performance in the DPS-MZI structure strongly depends on the type of waveguide core material and the wavelength applied. Si and InGaAsP have proven to be the most suitable materials for DPS-MZI structures, both for applications in the visible and infrared light spectra. Although $LiNbO_3$ exhibits higher propagation losses, it remains promising for high-speed modulator applications due to its significant electro-optic coefficient. Conversely, PMMA shows very low optical field confinement, resulting from its low refractive index contrast. This makes PMMA less suitable for DPS-MZI applications that require sharp interference and low propagation losses. Furthermore, an increase in wavelength tends to cause broader optical modes, particularly in materials with low refractive index contrast. Therefore, the selection of the waveguide core material and wavelength is a critical factor in designing and optimizing DPS-MZI-based photonic devices, especially for applications demanding stable and efficient light propagation.

REFERENCES

Akbulut, M., Kotov, L., Wiersma, K., Zong, J., Li, M., Miller, A., Chavez-Pirson, A., & Peyghambarian, N. (2021). An eye-safe, SBS-free coherent fiber laser LIDAR transmitter with millijoule energy and high average power. In *Photonics* (Vol. 8, No. 1, p. 15). MDPI.

Alsaad, A., Al Dairy, A. R., Ahmad, A., Qattan, I. A., Al Fawares, S., & Al-Bataineh, Q. (2021). Synthesis and characterization of polymeric (PMMA-PVA) hybrid thin films doped with TiO2 nanoparticles using dip-coating technique. *Crystals*, *11*(2), 99.

Alzamil, A. K., Sharawy, M. A., Almohimmah, E. M., Ragheb, A. M., Almaiman, A., & Alshebeili, S. A. (2024). Development of an Integrated Communication and Sensing System Using Spread Spectrum and Photonics Technologies. In *Photonics* (Vol. 11, No. 9, p. 861). MDPI.

Amin, R., Maiti, R., George, J. K., Ma, X., Ma, Z., Dalir, H., Miscuglio, M., & Sorger, V. J. (2020). A lateral MOS-capacitor-enabled ITO Mach–Zehnder modulator for beam steering. *Journal of Lightwave Technology*, *38*(2), 282-290.

Butt, M. A. (2024). Integrated optics: conventional Mach–Zehnder interferometer configuration versus loop terminated Mach–Zehnder interferometer configuration–a perspective. *Journal of optics*, *26*(10), 102501.

Chen, G., Yu, Y., Shi, Y., Li, N., Luo, W., Cao, L., Danner A. J., Liu A. Q., & Zhang, X. (2022). High-Speed Photodetectors on Silicon Photonics Platform for Optical Interconnect. *Laser & Photonics Reviews*, 16(12), 2200117.

Di Francescantonio, A., Sabatti, A., Weigand, H., Bailly-Rioufreyt, E., Vincenti, M. A., Carletti, L., Kellner, J., Zilli, A., Finazzi, M., Celebrano, M., & Grange, R. (2025). Efficient GHz electro-optical modulation with a nonlocal lithium niobate metasurface in the linear and nonlinear regime. *Nature Communications*, *16*(1), 7000.

Dong, J., Sang, M., Wang, S., Xu, T., Wang, Y., & Liu, T. (2020). A novel Mach–Zehnder interferometric temperature sensor based on a symmetrical double-grooved structure. *IEEE Sensors Journal*, *20*(24), 14850-14856.

Dong, S., Koh, D. M. Z., Martinelli, F., Brosseau, P. J., Petrović, M., Shen, L., Adamo, G., Vetlugin, A. N., Sidorova, M., Kurtsiefer, C., & Soci, C. (2024). Establishing an end-to-end workflow for SNSPD fabrication and characterization. *Scientific Reports*, *14*(1), 30891.

Fedotova, A., Carletti, L., Zilli, A., Setzpfandt, F., Staude, I., Toma, A., Finazzi M, De Angelis, C., Pertsch T., Neshev, D. N., & Celebrano, M. (2022). Meta-Optics with Lithium Niobate. *arXiv preprint arXiv:2211.00359*.

Hiraki, T., Aihara, T., Fujii, T., Takeda, K., Kakitsuka, T., Tsuchizawa, T., & Matsuo, S. (2020). Membrane InGaAsP Mach–Zehnder modulator integrated with optical amplifier on Si platform. *Journal of Lightwave Technology*, *38*(11), 3030-3036.

Horvath, T., Radil, J., Munster, P., & Bao, N. H. (2020). Optical amplifiers for access and passive optical networks: A tutorial. *Applied Sciences*, *10*(17), 5912.

Huang, W. T., Hsiao, F. H., Miao, W. C., Chang, C. T., Hong, K. B., Sher, C. W., Hong, Y. H., Lin. G. R., & Kuo, H. C. (2025). Emerging Modulator Technologies in Silicon Photonics. *IEEE Nanotechnology Magazine*.

Islam, A., & Ahmed, M. (2020). Study of attenuation and bending losses in signal transmission over step index multimode PMMA fibers. *Int J Ambient Syst Appl*, *8*.

Karabchevsky, A., & Choudhary, A. (Eds.). (2024). *On-Chip Photonics: Principles, Technology and Applications*. Elsevier.

Kazanskiy, N. L., Khonina, S. N., & Butt, M. A. (2022). Advancement in silicon integrated photonics technologies for sensing applications in near-infrared and mid-infrared region: a review. In *Photonics* (Vol. 9, No. 5, p. 331). MDPI.

Kim, Y., Bang, D. J., Kim, Y., & Kim, K. H. (2020). Magneto-optical properties of spin-coated bismuth-substituted yttrium iron garnet films on silicon substrates at 1550-nm wavelength. *AIP Advances*, *10*(2).

Li, Y., Fei, H., Liu, X., & Lin, H. (2025). Design of Refractive Index Sensors Based on Valley Photonic Crystal Mach–Zehnder Interferometer. *Sensors*, *25*(11), 3289.

Lorenz, L., & Bock, K. (2022). Current Development in the Field of Optical Short-Range Interconnects. In *Optical Polymer Waveguides: From the Design to the Final 3D-Opto Mechatronic Integrated Device* (pp. 1-13). Cham: Springer International Publishing.

Moatlhodi, O. O. (2022). *Vertical Cavity Surface Emitting Laser for Optical Communication Systems* (Master's thesis, Botswana International University of Science and Technology (Botswana)).

Modi, K. S., Kaur, J., Singh, S. P., Tiwari, U., & Sinha, R. K. (2020). Extremely high figure of merit in all-dielectric split asymmetric arc metasurface for refractive index sensing. *Optics Communications*, *462*, 125327.

Mulkerns, N. M., Hoffmann, W. H., Ramos-Soriano, J., de la Cruz, N., Garcia-Millan, T., Harniman, R. L., Lindsay, I. D., Seddon, A. M., Galan, M. C., & Gersen, H. (2022). Measuring the refractive index and sub-nanometre surface functionalisation of nanoparticles in suspension. *Nanoscale*, *14*(22), 8145-8152.

Nagar, M. A., & Janner, D. (2024). Polymer-Based Optical Guided-Wave Biomedical Sensing: From Principles to Applications. In *Photonics* (Vol. 11, No. 10, p. 972). MDPI AG.

Pan, P., Wen, J., Zha, S., Cai, X., Ma, H., & An, J. (2021). Fabrication and error analysis of a InGaAsP/InP polarization beam splitter based on an asymmetric Mach-Zehnder interferometer. *Optical Materials*, *118*, 111250.

Poon, J. K., Govdeli, A., Sharma, A., Mu, X., Chen, F. D., Xue, T., & Liu, T. (2024). Silicon photonics for the visible and near-infrared spectrum. *Advances in Optics and Photonics*, *16*(1), 1-59.

Prabu, R. T., Vignesh, G. D., Pandian, M. M., Dhandapani, A., Kumar, A. K., Sukumar, B., & Ali, Y. K. (2025). High speed optical modulation fiber systems for ultra high spectral efficiency improvement through the digital shift keying techniques employment. *Journal of Optical Communications*.

Saxena, P., & Shukla, P. (2022). A comparative analysis of the basic properties and applications of poly (vinylidene fluoride)(PVDF) and poly (methyl methacrylate)(PMMA). *Polymer Bulletin*, *79*(8), 5635-5665.

Siew, S. Y., Li, B., Gao, F., Zheng, H. Y., Zhang, W., Guo, P., Xie, S. W., Song, A., Dong, B., Luo, L. W., & Lo, G. Q. (2021). Review of silicon photonics technology and platform development. *Journal of Lightwave Technology*, *39*(13), 4374-4389.

Sohn, I., Jang, Y. H., & Lee, S. H. (2020). Ultra-low-power implantable medical devices: Optical wireless communication approach. *IEEE Communications Magazine*, *58*(5), 77-83.

Sun, Z., Li, Y., Bai, B., Zhu, Z., & Sun, H. (2022). Silicon nitride-based Kerr frequency combs and applications in metrology. *Advanced Photonics*, *4*(6), 064001.

Tsuda, H. (2020). Silicon photonics platforms for optical communication systems, outlook on future developments. *IEICE Electronics Express*, *17*(22), 20202002-20202002.

Tu, H., Liu, J., Dai, X., Weng, H., Li, N., Li, G., Lu, Q., Huang, L., Donegan, J., & Guo, W. (2025). Broadband electro-optic frequency comb with electrical and optical dual-resonance enhancement in lithium niobate. *Optics Express*, *33*(6), 13401-13412.

Vyas, K., Espinosa, D. H., Hutama, D., Jain, S. K., Mahjoub, R., Mobini, E., Awan, K. M., Lundeen, J., & Dolgaleva, K. (2022). Group III-V semiconductors as promising nonlinear integrated photonic platforms. *Advances in Physics: X*, *7*(1), 2097020.

Wang, T., Qiao, M., Liu, Y., Liu, T., & Xu, S. (2020). SrTiO3 optical waveguides fabricated by carbon ion irradiation at various fluences. *Optics Communications*, *474*, 126168.

Wang, Z., Cai, Y., Jiang, H., Tian, Z., & Di, Z. (2024). Graphene-based silicon photonic devices for optical interconnects. *Advanced Functional Materials*, *34*(9), 2307461.

Yang, Q., Zhou, L., Li, R., Liu, S., Lv, L., Chen, S., Ren S, Wang G, & Shen, C. (2024). Curvature sensing via symmetric fiber ball MZI and neural network with sparse data. *Optical Fiber Technology*, *85*, 103800.

Yu, Y., Yu, Z., Wang, L., & Sun, X. (2021). Ultralow-loss etchless lithium niobate integrated photonics at near-visible wavelengths. *Advanced Optical Materials*, *9*(19), 2100060.

Zhan, J., Li, Y., Luo, Z., & Liu, M. (2021). Topological design of multi-material compliant mechanisms with global stress constraints. *Micromachines*, *12*(11), 1379.

Zhou, X., Yi, D., Chan, D. W. U., & Tsang, H. K. (2024). Silicon photonics for high-speed communications and photonic signal processing. *npj Nanophotonics*, *1*(1), 27.

Zhu, B., Lei, S., Hu, M., Zhang, L., Yang, H., Xu, J., & Zhang, H. (2025). Tunable asymmetric Mach-Zehnder interferometer based on spoof surface plasmon polaritons. *Optics Express*, *33*(7), 15712-15723.